Geochemical Perspectives Letters



# Abiogenesis not required to explain the origin of volcanic-hydrothermal hydrocarbons

**J. Fiebig, A. Stefánsson, A. Ricci, F. Tassi, F. Viveiros, C. Silva, T.M. Lopez, C. Schreiber, S. Hofmann, B.W. Mountain**

## Supplementary Information

The Supplementary Information includes:



### *1. Methods*

Well fluids, well steam and natural gas discharges were sampled following standard protocols for fumaroles (Giggenbach, 1975; Cioni and Corazza, 1981) and bi-phase well discharges (Arnórsson *et al.* 2006). A variety of analytical setups was used to analyse the stable isotopic composition of *n*-alkanes, $CO_2$ and water. Carbon isotope analysis of *n*-alkanes and $CO_2$ were performed using analytical setups described by Fiebig *et al.* (2015). For hydrogen isotope analysis of $CH_4$, a sample preconcentration system was connected to a GC/TC (Thermo Finnigan), equipped with a Porapack Q column. $CH_4$ was separated from $H_2$ by keeping the column isothermal at –50 °C and finally introduced into a MAT 253 gas source mass spectrometer (Thermo Finnigan) using He as a carrier gas. The hydrogen isotopic composition of water was analysed using a TC-EA (Thermo Finnigan). Raw isotopic data were corrected analysing isotopic reference materials (whose known isotopic compositions bracket those of the samples) along with the samples, following the principle of identical treatment of sample and reference materials (*e.g.*, Meier-Augenstein and Schimmelmann, 2019). Methane#1, methane#3, ALM methane#7 (all supplied by A. Schimmelmann, Indiana University) and two inhouse $CH_4$ standards (calibrated against methane #1, #3 and #7) were used for the correction of raw $\delta^{13}C_{1\text{-}4}$ and raw $\delta^{2}H\text{-}C_1$, three inhouse $CO_2$ gases anchored on the VPDB-LSVEC for the correction of raw $\delta^{13}CO_2$, and three inhouse water samples calibrated on the VSMOW-SLAP scale for the correction of raw $\delta^{2}D\text{-}H_2O$. External precision for carbon isotope analysis was ±0.5 ‰ for *n*-alkanes

and ±0.2 ‰ for $CO_2$. External precisions for $\delta^2H$ analysis of $CH_4$ and $H_2O$ were ≤±5 ‰ and ≤±3 ‰, respectively. All isotopic data are presented in Tables S-2 (wells) and S-3 (fumaroles).

## 2. Sampled Locations

Information about the major characteristics of each sampled site, with respect to tectonic setting, host rocks and the source of water feeding the corresponding hydrothermal system at depth is provided in Table S-1 (see references there for further reading). Tables S-2 and S-3 list the carbon and hydrogen isotopic compositions of *n*-alkanes in well discharges and fumaroles, respectively, as well as the hydrogen isotopic compositions of discharged water vapour and liquid water.

## 3. Data Modelling

### 3.1. Temperature dependence of the hydrogen isotope fractionation between $H_2O_{(v)}$ and $CH_4$

For a given temperature between 200 °C and 400 °C (Figs. S-2, S-4), the hydrogen isotope fractionation between water vapour and methane ($\alpha_{H_2O\text{-}CH_4}$) can be computed from the hydrogen isotope fractionations between water vapour and $H_2$ ($\alpha_{H_2O\text{-}H_2}$) and $CH_4$ and $H_2$ ($\alpha_{CH_4\text{-}H_2}$) according to

$$\alpha_{H_2O\text{-}CH_4} = \alpha_{H_2O\text{-}H_2} / \alpha_{CH_4\text{-}H_2} \quad \text{(Eq. S-1)}$$

Temperature dependencies for $\alpha_{H_2O\text{-}H_2}$ were determined experimentally by Suess (1949) and theoretically by Bardo and Wolfsberg (1976), whereas the temperature dependence of $\alpha_{CH_4\text{-}H_2}$ was experimentally constrained by Horibe and Craig (1995). Note that values of +2 ‰, –6 ‰, –17 ‰, –30 ‰ and –39 ‰ must finally be added to values of $1000*\ln(\alpha_{H2O\text{-}CH4})$ at temperatures of 200 °C, 250 °C, 300 °C, 350 °C and 400 °C, respectively, to account for polymerisation of water vapour monomers at temperatures ≥200 °C (Driesner, 1997).

### 3.2. Modelling of open system cracking of organic matter

A variety of parameters controls the carbon and hydrogen isotopic composition of gaseous *n*-alkanes deriving from the thermal decomposition of organic matter. Amongst these are temperature, the initial isotopic composition of the parental organic matter, site specific isotope fractionations inside the parental organic matter (as each *n*-alkane can be derived from different precursor sites within), the degree of cracking and open *vs* closed system degassing (Clayton, 1991; Rooney *et al.*, 1995; Berner *et al.*, 1995; Lorant *et al.*, 1998). Both pyrolysis experiments and theoretical computations provided evidence that the apparent carbon isotope fractionation between a given precursor site in the organic matter and the evolving gaseous *n*-alkane decreases with the number of carbon atoms constituting the *n*-alkane and with temperature (Clayton, 1991; Berner *et al.*, 1995; Tang *et al.*, 2000). If site-specific isotope fractionations within the organic matter can be neglected, generated *n*-alkanes can, therefore, be expected to approach the carbon isotopic composition of the initial source material with increasing chain length and with increasing temperature (Chung *et al.*, 1988). Upon degassing, the different precursor sites inside the organic matter will, however, change their isotopic compositions differently, depending on the magnitude of isotope fractionation between a given *n*-alkane and its corresponding precursor site, the mode of gas generation (closed *vs.* open system) and the fraction of *n*-alkane generated (Clayton, 1991; Rooney *et al.*, 1995). For a given *n*-alkane precursor site, the effect of open system cracking on its bulk carbon isotopic composition can be modelled using equation (3) of Clayton (1991):

$$\delta^{13}C_{PS} = (1000 + \delta^{13}C_I) * f_{PS}^{(\alpha_C - 1)} - 1000 \quad \text{(Eq. S-2)}$$

where $\delta^{13}C_{PS}$ is the carbon isotopic composition of the precursor site specific for a given *n*-alkane inside the organic matter, $\delta^{13}C_I$ the initial carbon isotopic composition of the specific precursor site, $\alpha_C$ the carbon isotope fractionation factor between a given *n*-alkane and its precursor site and $f_{PS}$ the fraction of residual precursor sites. Further, it is

$$f_{PS} = 1 - f_{n\text{-alk}} \quad \text{(Eq. S-3)}$$

and

$$\delta^{13}C_{n\text{-alk}} = \alpha_C * (1000 + \delta^{13}C_{PS}) - 1000 \quad \text{(Eq. S-4)}$$

where $f_{n\text{-alk}}$ is the fraction of *n*-alkane generated and $\delta^{13}C_{n\text{-alk}}$ the carbon isotopic composition of the corresponding instantaneously generated fraction of *n*-alkane. Insertion of (Eq. S-2) and (Eq. S-3) in (Eq. S-4) yields

$$\delta^{13}C_{n\text{-alk}} = \alpha_C * (1000 + \delta^{13}C_I) * (1 - f_{n\text{-alk}})^{(\alpha_C - 1)} - 1000 \qquad \text{(Eq. S-5)}$$

***3.2.1. Modelling the carbon isotopic compositions of instantaneously generated fractions of methane, ethane and propane.*** Equation S-5 can be used to model the evolution of the carbon isotopic composition of a given n-alkane as a function of the fraction of *n*-alkane generated (Figs. S-3a,b,c). See there for more specific details on α-values and $\delta^{13}C_I$ chosen for data modelling.

***3.2.2. Modelling the carbon and hydrogen isotopic compositions of instantaneously generated fractions of methane.*** The carbon and hydrogen isotopic compositions of instantaneously generated fractions of methane have been modelled as a function of the fraction of residual precursor sites for open system cracking of both marine and terrestrial organic matter in Figure 2a. In analogy to Equation S-5, the following equations were used for this purpose:

$$\delta^{13}C_{CH_4} = \alpha_C * (1000 + \delta^{13}C_{(CH_4)I}) * f_{PS(CH_4)}^{(\alpha_C - 1)} - 1000 \qquad \text{(Eq. S-6)}$$

$$\delta^{2}H_{CH_4} = \alpha_H * (1000 + \delta^{2}H_{(CH_4)I}) * f_{PS(CH_4)}^{(\alpha_H - 1)} - 1000 \qquad \text{(Eq. S-7)}$$

For open system cracking of marine organic matter, $\alpha_C$ and $\alpha_H$ were set to 0.983 and 0.909, respectively (as constrained from pyrolysis experiments of marine kukersite; Berner *et al.* 1995), and the initial isotopic composition of methane precursor sites ($\delta^{13}C_{(CH_4)I}$, $\delta^{2}H_{(CH_4)I}$) was assumed to be identical to the average isotopic composition of marine organic matter ($\delta^{13}C$ = –20 ‰, $\delta^{2}H$ = –100 ‰; Schoell, 1984). For open system cracking of terrestrial organic matter, $\alpha_C$ and $\alpha_H$ were set to 0.9958 and 0.8333, respectively (as constrained from pyrolysis experiments of terrestrial xylite, Berner *et al.*, 1995), and the initial isotopic composition of methane precursor sites ($\delta^{13}C_{(CH_4)I}$, $\delta^{2}H_{(CH_4)I}$) was assumed to be identical to the average isotopic composition of $C_3$ plants ($\delta^{13}C$ = –28 ‰, $\delta^{2}H$ = –100 ‰; Schoell, 1984).

## *4. Additional Data (Displayed in Figures)*

Figures 1c and 2c also show the isotopic composition of n-alkanes previously identified to be abiotic in origin. These include data from (ultra)mafic hydrothermal systems (Lost City: Proskurowski *et al.* (2006), unsedimented mid-ocean ridges: McCollom and Seewald (2007), Socorro: Taran *et al.* (2010)), continental volcanic-hydrothermal systems (Milos: Botz *et al.* (1996)), ophiolites (Zambales: Abrajano *et al.* (1988), Chimaera: Etiope *et al.* (2011), inclusions in igneous rocks (Khibina: Potter *et al.* (2004), Potter and Longstaffe (2007), Lovozero: Potter *et al.* (2004)), old cratons (Kidd Creek, Driefontein, Kloof, Copper Cliff, Mponeng: all Sherwood Lollar *et al.* (2006), Sudbury, Elliott Lake, Red Lake, Juuka, Pori: all Sherwood Lollar *et al.* (1993)) and from cold (hyper)alkaline springs (Al Khoud Nizwa: Fritz *et al.* (1992), Genova: Boschetti *et al.* (2013), Othrys: Etiope *et al.* (2013a), Cabeco de Vide: Etiope *et al.* (2013b), Happo: Suda *et al.* (2014), Al Farfar: Etiope *et al.* (2015), Ronda: Etiope *et al.* (2016)). Craton gases and (hyper)alkaline spring gases with a predominant microbial contribution were excluded, as was previously done in the correlation plots of $\delta^{2}H$-$CH_4$ *vs.* $\delta^{13}C$-$CH_4$ compiled by Etiope and Sherwood Lollar (2013) and Etiope (2017).

## *Supplementary Tables*

**Table S-1** The major characteristics of the investigated volcanic-hydrothermal systems.

| Country | Geothermal system | Tectonic setting | Rocks | $T_{res}$[a] (°C) | Source of external waters[b] | References |
|---|---|---|---|---|---|---|
| *Alaska, USA* | | subduction | | | | |
| | Trident | | andesitic, dacitic | 380 | MW | Lopez *et al.* (2017) |
| | Mageik | | andesitic, dacitic | 260 | MW | Lopez *et al.* (2017) |
| *Argentina* | | subduction | | | | |
| | Domuyo | | andesitic, rhyolitic | 220-240 | MW | Tassi *et al.* (2016) |
| | Copahue | | basaltic-andesitic, dacitic | 250 | MW | Tassi *et al.* (2017) |
| *Azores, Portugal* | | mid-ocean rifting/mantle plume | | | | |
| | Furnas | | trachyte | 200-275 | MW | Caliro *et al.* (2015), Moore (1990) |
| *Greece* | | subduction | | | | |
| | Nisyros | | andesitic, dacitic, rhyolitic | 290-340 | SW | Chiodini *et al.* (1993), Brombach *et al.* (2003) |
| | Santorini | | andesitic, dacitic, rhyolitic | unknown | unknown | Fytikas *et al.* (1989) |
| *Iceland* | | mid-ocean rifting/mantle plume | | | | |
| | Reykjanes | | basalts | 260-345 | SW | Stefánsson *et al.* (2017) |
| | Svartsengi | | basalts | 220-260 | SW+MW | Stefánsson *et al.* (2017) |
| | Krýsuvík | | basalts | 220-320 | MW | Stefánsson *et al.* (2017) |
| | Krafla | | basalts, ryolites | 200-440 | MW | Stefánsson *et al.* (2017) |
| | Námafjall | | basalts, ryolites | 220-320 | MW | Stefánsson *et al.* (2017) |
| | Hengill | | basalts | 200-380 | MW | Stefánsson *et al.* (2017) |
| | Hveragerdi | | basalts | 170-230 | MW | Stefánsson *et al.* (2017) |
| | Torfajökull | | rhyolites | 260-310 | MW | Stefánsson *et al.* (2017) |
| | Kverkfjöll | | rhyolites | 260-300 | MW | Stefánsson *et al.* (2017) |
| | Kverkfjöll | | basalts, rhyolites | 290-350 | MW | Stefánsson *et al.* (2017) |
| | Askja | | basalts, rhyolites | 180-350 | MW | Stefánsson *et al.* (2017) |
| *Italy* | | subduction | | | | |
| | Vulcano beach | | leucite tephrites, trachytes, alkali-rhyolites | 230 | SW+MW | Chiodini *et al.* (1995), Keller (1980) |
| | Ischia | | shoshonites, alkalitrachytes | 250-300 | MW | Panichi *et al.* (1992), Chiodini *et al.* (2004) |
| | C. Flegrei | | shoshonite, phonolites, trachytes | 200-360 | MW | Caliro *et al.* (2007, 2014) |
| | Vesuvio | | leucite-basalts, trachytes, leucitic tephrites, leucitic phonolites | 360-450 | MW | Chiodini *et al.* (2001) |
| | Pantelleria | continental extensional | trachytes, peralalkaline rhyolites | 250 | MW | Parello *et al.* (2000) |

**Table S-1** continued

| Country | Geothermal system | Tectonic setting | Rocks | $T_{res}$[a] (°C) | Source of external waters[b] | References |
|---|---|---|---|---|---|---|
| *New Zealand* | | subduction | | | | |
| | Ohaaki | | rhyolites, greywacke | 275-310 | MW | Giggenbach (1995), Christenson *et al.* (2002) |
| | Rotokawa | | andesites, dacites, rhyolites, greywacke | 290-340 | MW | Giggenbach (1995), Sewell *et al.* (2015) |
| | Ngatamariki | | basalt, andesite, rhyolite, greywacke, tonalite | 260-285 | MW | Giggenbach (1995), Chambefort *et al.* (2016) |
| *Tenerife, Spain* | | | | | | |
| | Teide | mantle plume | basalt, trachytes, phonolites | 285-316 | MW | Melian *et al.* (2012) |

[a] reservoir temperature either measured directly or inferred from gas concentration geothermometers; [b] origin inferred from oxygen and hydrogen isotope data [see references]

**Table S-2** Well data: Reservoir temperatures, sampling temperatures, carbon isotope composition of methane, ethane, propane and *n*-butane, hydrogen isotope composition of methane, steam and liquid water. Carbon and hydrogen isotope data are reported in ‰-deviation relative to VPDB and VSMOW, respectively.

| Sample # | Location | Date | $T_{res}$[a] (°C) | $T_s$[b] (°C) | $\delta^{13}C$-$CH_4$ | $\delta^{2}H$-$CH_4$ | $\delta^{13}C$-$C_2H_6$ | $\delta^{13}C$-$C_3H_8$ | $\delta^{13}C$-*n*-$C_4H_{10}$ | $\delta^{13}C$-$CO_2$(v) | $\delta^{2}H$-$H_2O$(v) | $\delta^{2}H$-$H_2O$(l) |
|---|---|---|---|---|---|---|---|---|---|---|---|---|
| | *Iceland* | | | | | | | | | | | |
| Kr w32 | Krafla | 27/08/2015 | 249 | 178 | -39.4 | -314 | -33.9 | -28.4 | -24.9 | -3.8 | -82 | -84 |
| Kr w16 | Krafla | 27/08/2015 | 264 | 203 | -37.6 | -239 | -36.4 | -32.3 | | -3.5 | -83 | -90 |
| Kr w34 | Krafla | 28/08/2015 | 264 | 200 | -37.5 | -220 | -28.4 | -24.2 | | -4.2 | -82 | -86 |
| Kr w34 | Krafla | 06/08/2016 | 264 | 200 | -36.3 | -226 | -32.9 | -24.7 | -22.1 | -4.3 | -81 | -83 |
| Kr w37 | Krafla | 06/08/2016 | 295 | 175 | -38.2 | -251 | -35.3 | -27.3 | -27.1 | -4.2 | -83 | |
| Kr w31 | Krafla | 06/08/2016 | 297 | 148 | -36.6 | -224 | -27.9 | -18.3 | | -3.4 | -82 | |
| Kr w36 | Krafla | 06/08/2016 | 241 | 189 | -34.0 | -233 | -32.8 | -25.3 | | -4.8 | -83 | -86 |
| Kr w27 | Krafla | 06/08/2016 | 243 | 183 | -39.0 | -293 | -34.8 | -24.7 | -23.2 | -2.9 | -83 | -83 |
| Rey w15 | Reykjanes | 02/09/2015 | 281 | 212 | -31.5 | -162 | -18.1 | -19.0 | -20.0 | -2.8 | -28 | -12 |
| Rey w12 | Reykjanes | 02/09/2015 | 299 | 220 | -29.6 | -150 | -17.1 | -17.3 | -18.3 | -2.8 | -26 | -23 |
| Rey w12 | Reykjanes | 12/08/2016 | 299 | 207 | -29.3 | -152 | -17.6 | -17.0 | -16.9 | -3.0 | -27 | -20 |
| Rey w18 | Reykjanes | 12/08/2016 | 277 | 217 | -32.0 | -172 | -19.7 | -22.0 | -23.3 | -2.6 | -27 | -22 |
| Rey w11 | Reykjanes | 12/08/2016 | 305 | 226 | -24.6 | -138 | -16.2 | -15.9 | -15.9 | -3.0 | -24 | -20 |
| Nam w13 | Námafjall | 27/08/2015 | 290 | 173 | -37.2 | -259 | -32.1 | -25.0 | | -3.7 | -95 | -93 |
| Nam w13 | Námafjall | 05/08/2016 | 285 | 126 | -36.1 | -263 | -32.2 | -25.0 | | -3.9 | -98 | -90 |
| Nam w9 | Námafjall | 27/08/2015 | 236 | 184 | -35.4 | -288 | -35.1 | -23.9 | -22.2 | -3.0 | -89 | -95 |
| Nam w9 | Námafjall | 05/08/2016 | 234 | 175 | -34.8 | -283 | -34.8 | -22.9 | -20.9 | -3.2 | -89 | -94 |
| Sv w9 | Svartsengi | 11/08/2016 | 240 | 192 | -30.4 | -188 | -18.7 | -18.9 | -19.4 | -2.3 | -29 | -20 |
| Sv w11 | Svartsengi | 11/08/2016 | 240 | 204 | -30.6 | -183 | -17.9 | -17.3 | -17.7 | -2.8 | -28 | -19 |
| | *New Zealand* | | | | | | | | | | | |
| BR 67 | Ohaaki | 01/03/2017 | 304 | 192 | -26.0 | -140 | -20.5 | -20.2 | | -7.6 | -45 | -39 |
| BR 56 | Ohaaki | 01/03/2017 | 268 | 174 | -26.4 | -142 | -22.5 | -23.7 | -25.9 | -6.9 | -45 | -39 |

**Table S-2** continued

| Sample # | Location | Date | $T_{res}$[a] (°C) | $T_s$[b] (°C) | $\delta^{13}C$-$CH_4$ | $\delta^{2}H$-$CH_4$ | $\delta^{13}C$-$C_2H_6$ | $\delta^{13}C$-$C_3H_8$ | $\delta^{13}C$-$n$-$C_4H_{10}$ | $\delta^{13}C$-$CO_2$(v) | $\delta^{2}H$-$H_2O$(v) | $\delta^{2}H$-$H_2O$(l) |
|---|---|---|---|---|---|---|---|---|---|---|---|---|
| BR 49 | Ohaaki | 01/03/2017 | 289 | 177 | -25.3 | -142 | -22.2 | -21.4 | | -7.2 | -45 | -39 |
| RK 26 | Rotokawa | 02/03/2017 | 293 | 248 | -25.1 | -144 | -25.0 | -28.1 | -27.8 | -5.5 | -43 | -44 |
| RK 34 | Rotokawa | 02/03/2017 | 289 | 245 | -25.3 | -140 | -15.6 | -17.5 | -17.1 | -7.3 | -41 | -44 |
| RK 14 | Rotokawa | 02/03/2017 | 316 | 236 | -25.8 | -141 | -26.5 | -26.9 | -26.9 | -6.6 | -44 | -42 |
| RK 17 | Rotokawa | 02/03/2017 | 300 | 245 | -25.4 | -142 | -19.8 | -21.2 | -22.7 | -5.8 | -45 | -44 |
| NM 5 | Ngatamarigi | 03/03/2017 | 287 | 216 | -25.5 | -147 | -22.5 | -21.5 | -21.3 | -6.4 | -42 | -40 |
| NM 7 | Ngatamarigi | 03/03/2017 | 287 | 224 | -25.0 | | | | | -6.0 | -46 | -42 |
| NM 12 | Ngatamarigi | 03/03/2017 | 284 | 224 | -24.8 | -146 | -22.0 | -18.3 | -17.8 | -5.8 | -43 | -43 |

[a] $T_{res}$ = reservoir temperature calculated assuming adiabatic boiling and using quartz geothermometry; [b] $T_s$ = Sampling temperature;

**Table S-3** Fumarole data: Vent temperatures, carbon isotope composition of methane, ethane, propane and *n*-butane, hydrogen isotope composition of methane and water vapour. Carbon and hydrogen isotope data are reported in ‰-deviation relative to VPDB and VSMOW, respectively.

| Sample | Location | Date | $T_v$[a] (°C) | $\delta^{13}C$-$CH_4$ | $\delta^{2}H$-$CH_4$ | $\delta^{13}C$-$C_2H_6$ | $\delta^{13}C$-$C_3H_8$ | $\delta^{13}C$-*n*-$C_4H_{10}$ | $\delta^{13}C$-$CO_2$(v) | $\delta^{2}H$-$H_2O$(v) |
|---|---|---|---|---|---|---|---|---|---|---|
| | ***Italy*** | | | | | | | | | |
| Vasca Ippo | Vulcano | Jun 16 | | -5.2 | -82 | -22.3 | -26.1 | -26.3 | -2.9 | -9 |
| Vasca Ippo Centr. | Vulcano | 04/10/16 | 102 | -5.4 | -84 | -24.4 | -24.6 | -25.3 | -3.2 | -9 |
| Vasca Ippo Est. | Vulcano | 04/10/16 | 100 | -5.2 | -84 | -20.1 | -23.3 | | -3.6 | -7 |
| Vasca Vecchia | Vulcano | 04/10/16 | 100 | -4.8 | -85 | -17.0 | | | -3.6 | -11 |
| FG | Pantelleria | 02/10/13 | 98 | -17.7 | -125 | -21.8 | | | -4.1 | -36 |
| Pisciarelli | C. Flegrei | 02/09/13 | 98 | -20.5 | -157 | -19.2 | | | -1.2 | -17 |
| BG | C. Flegrei | 02/09/13 | 163 | -17.2 | -143 | -17.8 | | | -1.2 | -21 |
| BN | C. Flegrei | 02/09/13 | 157 | -18.5 | -142 | -17.8 | | | -0.8 | -26 |
| FC2 | Vesuvio | 03/09/13 | 97 | -17.7 | -106 | -17.3 | | | 0.4 | -26 |
| DR2 | Ischia | 04/09/13 | 100 | -32.4 | -213 | -27.1 | -27.3 | -27.1 | -3.8 | -47 |
| | ***Greece*** | | | | | | | | | |
| S4 | Nisyros | 04/06/13 | 100 | -23.3 | -118 | -18.0 | -18.0 | -17.9 | -1.0 | -4 |
| S15 | Nisyros | 04/06/13 | 100 | -22.5 | -118 | -18.2 | -18.0 | | -1.0 | -6 |
| PP9S | Nisyros | 05/06/13 | 100 | -21.9 | -118 | -18.6 | -19.6 | | -0.3 | -7 |
| K7 | Nisyros | 06/06/13 | 99 | -22.5 | -119 | -18.4 | -18.4 | | -1.3 | -13 |
| A13 | Nisyros | 05/06/13 | 99 | -23.3 | -131 | -21.3 | -19.6 | -18.9 | -0.4 | 5 |
| Nea Kameni | Santorini | 06/04/16 | | -31.5 | | -26.0 | -20.8 | | | |
| | ***Tenerife*** | | | | | | | | | data from Melian *et al.* (2012) |
| FC | Teide | 16/06/13 | | -8.7 | -111 | -18.2 | | | -3.6 | -47 |
| | ***Azores*** | | | | | | | | | data from Caliro *et al.* (2015) |
| Furnas B | Furnas village | 06/01/15 | 65 | -64.7 | -309 | -30.7 | -29.9 | | | -25 |
| Furnas B | Furnas village | 24/07/15 | 74 | -63.1 | -304 | -31.3 | -30.7 | | -4.1 | -25 |
| Furnas B2 | Furnas village | 24/07/15 | 74 | -20.2 | -127 | -29.8 | -29.7 | | -4.1 | -25 |
| Furnas B3 | Furnas village | 24/07/15 | 98 | -19.4 | -125 | -29.0 | -29.4 | | -4.1 | -25 |
| Furnas D | Furnas village | 24/07/15 | 98 | -19.9 | -130 | -29.8 | -29.8 | | -4.2 | -25 |
| Esguicho | Furnas village | 28/11/13 | 95 | -17.9 | | -28.4 | -28.9 | -28.2 | -4.3 | -25 |
| Esguicho | Furnas village | 23/07/15 | 98 | -18.5 | -117 | -28.4 | -29.2 | | | -25 |
| Caldeira Seca | Furnas village | 28/11/13 | 99 | -18.7 | | -28.8 | -27.1 | -27.5 | -4.2 | -25 |
| Caldeira Seca | Furnas village | 06/01/15 | | -17.8 | -119 | -28.4 | -27.0 | | | -25 |
| Caldeira Seca | Furnas village | 23/07/15 | 97 | -19.5 | -126 | -28.8 | -27.5 | | -4.1 | -25 |

**Table S-3** continued

| Sample | Location | Date | $T_v$[a] (°C) | $\delta^{13}C$-$CH_4$ | $\delta^{2}H$-$CH_4$ | $\delta^{13}C$-$C_2H_6$ | $\delta^{13}C$-$C_3H_8$ | $\delta^{13}C$-$n$-$C_4H_{10}$ | $\delta^{13}C$-$CO_2$(v) | $\delta^{2}H$-$H_2O$(v) |
|---|---|---|---|---|---|---|---|---|---|---|
| Dos Vimes | Furnas village | 24/07/15 | 94 | -19.3 | -135 | -29.4 | -30.8 | | | -25 |
| Furnas Lake | Furnas lake | 28/11/13 | 97 | -35.9 | | -23.3 | -26.2 | | -4.8 | -23 |
| Furnas Lake | Furnas lake | 06/01/15 | 97 | -34.8 | -168 | -22.1 | | | | -23 |
| Furnas Lake | Furnas lake | 25/07/15 | 98 | -26.9 | -135 | -22.1 | -23.6 | | -4.5 | -23 |
| Furnas Lake 4 | Furnas lake | 25/07/15 | 96 | -27.4 | -138 | -22.1 | -23.8 | | -4.5 | -23 |
| Furnas Lake 2 | Furnas lake | 28/11/13 | 89 | -64.7 | | -24.8 | -26.8 | | -6.9 | -23 |
| Furnas Lake 2 | Furnas lake | 06/01/15 | 97 | -64.5 | -241 | -24.3 | | | | -23 |
| Furnas Lake 2 | Furnas lake | 25/07/15 | 93 | -63.3 | -238 | -24.0 | -26.5 | | -4.4 | -23 |
| | | | | | | | | | | |
| ***Iceland*** | ***Iceland*** | | | | | | | | | |
| 15-AS-01 | Krýsuvík | 24/08/15 | | -35.2 | -203 | -29.0 | -20.6 | | -3.2 | |
| 15-AS-02 | Krýsuvík | 24/08/15 | | -36.1 | -200 | -31.6 | | | | |
| 15-AS-03 | Kerlingafjöll | 25/08/15 | | -24.3 | -196 | -31.0 | | | -3.2 | |
| 15-AS 04 | Kerlingafjöll | 25/08/15 | | -24.3 | -195 | -30.7 | | | -3.3 | |
| 15-AS-05 | Kerlingafjöll | 26/08/15 | | -26.1 | -200 | -32.2 | | | -3.1 | |
| 15-AS-06 | Kerlingafjöll | 26/08/15 | | -25.6 | -196 | -32.5 | | | -3.0 | |
| 15-AS-11 | Námafjall | 28/08/15 | | -34.3 | -297 | -32.0 | -25.5 | | | |
| 16-AS-08 | Námafjall | 07/08/16 | | -33.5 | -265 | -24.2 | -21.8 | | -3.0 | -109 |
| 16-AS-09 | Námafjall | 07/08/16 | | -34.3 | -267 | -24.9 | -21.4 | | -3.2 | -108 |
| 16-AS-10 | Hengill | 09/08/16 | | -28.6 | -236 | -36.9 | -34.6 | | -3.6 | -65 |
| 16-AS-11 | Hveragerdi | 09/08/16 | | -32.8 | -252 | -41.8 | -29.9 | | -3.5 | -67 |
| 16-AS-12 | Hveragerdi | 09/08/16 | | -25.5 | -185 | -37.4 | -29.1 | -27.2 | -3.1 | -64 |
| 17-TORF-1 | Torfajökull | 07/08/17 | | -32.5 | -230 | -35.1 | -28.2 | -28.2 | -6.5 | |
| 17-TORF-2 | Torfajökull | 07/08/17 | | -30.6 | -210 | -32.9 | -25.5 | -30.6 | | |
| 17-KVE-1 | Kverkfjöll | 06/09/17 | | -33.6 | -226 | -44.1 | -29.9 | -24.2 | | |
| 17-KVE-2 | Kverkfjöll | 06/09/17 | | -33.9 | -219 | -43.5 | -30.5 | -24.8 | | |
| 17-ASK-1 | Askja | 07/09/17 | | -43.3 | -320 | -38.7 | -27.2 | | | |
| 17-ASK-3 | Askja | 07/09/17 | | -39.2 | -293 | -37.5 | | | | |
| | | | | | | | | | | |
| | ***Alaska*** | | | | | | | | | |
| MGK1 | Mageik | 12/07/13 | 92 | -30.5 | | -27.5 | -26.3 | -25.8 | -8.8 | |
| TRI1 | Trident | 16/07/13 | 94 | -20.2 | | -23.8 | -22.6 | | -11.0 | |

**Table S-3** continued

| Sample | Location | Date | $T_v$[a] (°C) | $\delta^{13}C$-$CH_4$ | $\delta^{2}H$-$CH_4$ | $\delta^{13}C$-$C_2H_6$ | $\delta^{13}C$-$C_3H_8$ | $\delta^{13}C$-$n$-$C_4H_{10}$ | $\delta^{13}C$-$CO_2$(v) | $\delta^{2}H$-$H_2O$(v) |
|---|---|---|---|---|---|---|---|---|---|---|
| | ***Argentina*** | | | | | | | | | |
| Bramadora | Domuyo | 01/03/14 | 107 | -29.6 | | -19.4 | -19.7 | | | |
| Anfiteatro | Copahue | 11/03/14 | 94 | -36.0 | | -23.4 | -18.3 | | -6.5 | |
| Las Maquintas | Copahue | 04/03/14 | 131 | -27.9 | | -21.7 | -18.3 | -18.2 | -7.6 | |
| Las Maquinas | Copahue | 04/03/14 | 94 | -26.4 | | -20.9 | -18.8 | | -7.6 | |
| Pedra de Copahue | Copahue | 06/03/14 | 93 | -27.0 | | -21.2 | -19.5 | | -7.5 | |
| Chancho-Co | Copahue | 07/03/14 | 95 | -29.6 | | -19.4 | | | -8.8 | |

[a] $T_v$ = Vent temperature

## *Supplementary Figures*

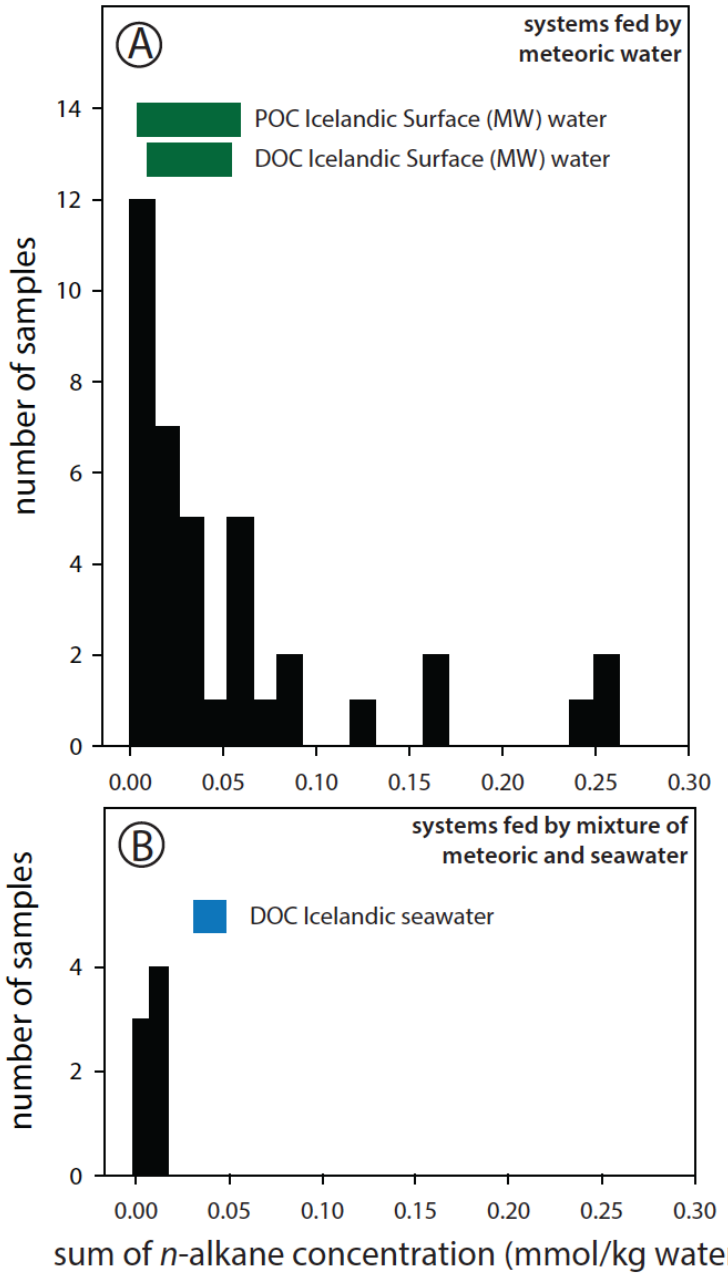


**Figure S-1** The concentration of *n*-alkanes in volcanic-hydrothermal fluids in Iceland. Systems sourced by **(a)** meteoric water and **(b)** a mixture of meteoric water and seawater. Also shown are the ranges of concentrations of DOC in non-thermal meteoric surface waters in Iceland (Eirkisdottir *et al.*, 2016; Chliffard *et al.*, 2018) and DOC and POC for seawater in Iceland (Fontela *et al.*, 2016). Total concentrations of *n*-alkanes (sum of methane, ethane, propane and *n*-butane) in the hydrothermal fluids are generally below the concentrations of organic matter in the source fluids. The volcanic-hydrothermal systems in Iceland are of recent geological age and characterised by the absence of organic sediments. For more complex systems, with multiple phase relationships (vapour, liquid, brine and halite) like sub-seafloor systems, and those associated with sedimentary deposits within the reservoir, mass balances are, however, difficult to constrain.

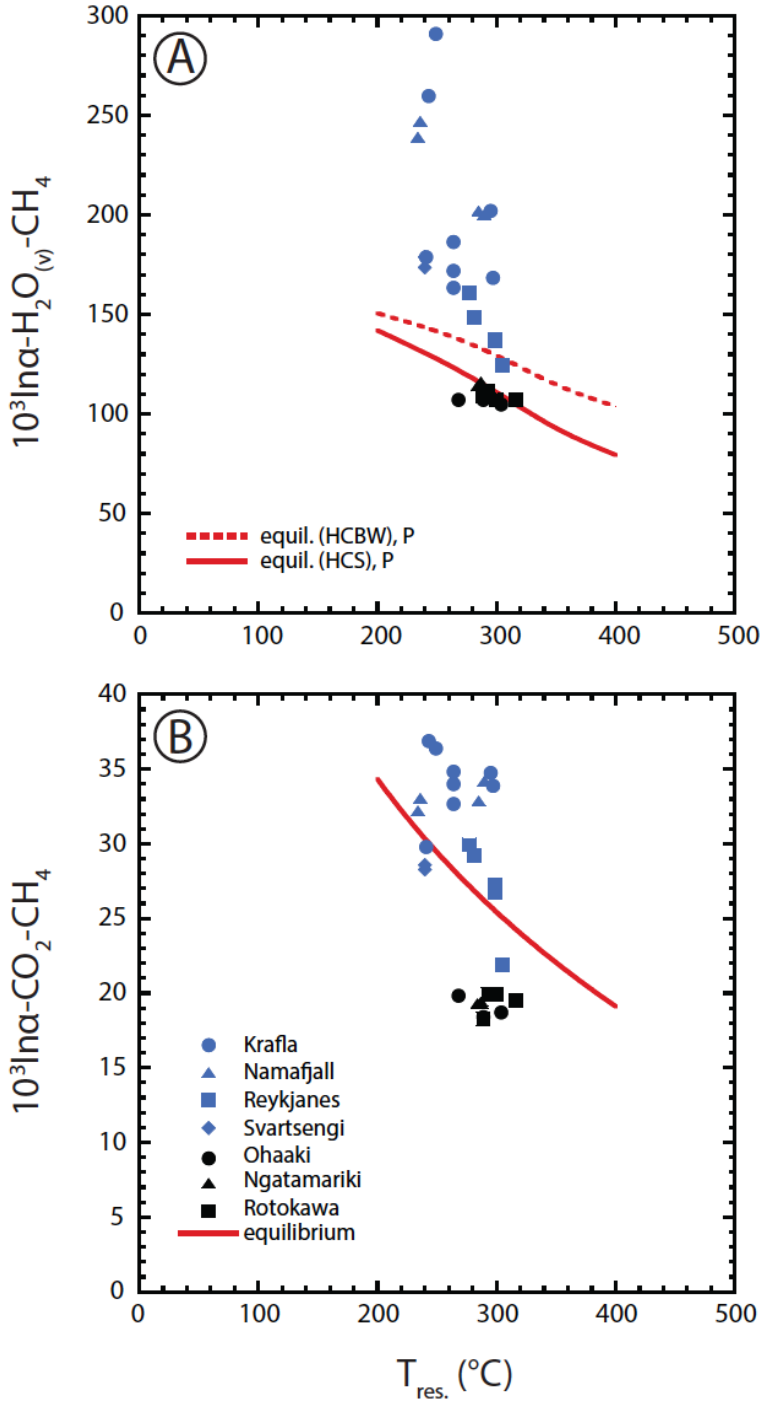


**Figure S-2** Apparent isotope fractionations *vs.* well reservoir temperatures. All well reservoir temperatures were determined from quartz-solute thermometry (Gunnarsson *et al.*, 2000). **(a)** 1000lnα($H_2O_{(v)}$-$CH_4$) *vs.* reservoir T. Hydrogen isotope equilibrium is marked by red lines. HCBW combines the theoretical $H_2$-$H_2O_{(v)}$ (Bardo and Wolfsberg, 1976) with the experimental $CH_4$-$H_2$ fractionation (Horibe and Craig, 1995), whereas HCS is based on a combination of the experimental $H_2$-$H_2O_{(v)}$ (Suess, 1949) with the experimental $CH_4$-$H_2$ fractionation (Horibe and Craig, 1995). Both the theoretical and experimental $H_2$-$H_2O_{(v)}$ fractionations were corrected for a density effect (Driesner, 1997) considering that gaseous water molecules above 200 °C do not behave ideal, but form polymers. For further information see Supplementary Information. The size of the markers roughly corresponds to analytical precisions of isotope analyses. Data implies that hydrogen isotope equilibrium between $CH_4$ and water is attained at highest reservoir temperatures of ≥300 °C. Isotope fractionation associated with steam separation seems to be of minor importance only since the hydrogen isotopic composition of the steam always corresponds to that of the discharged liquid water (Table S-2). **(b)** 1000lnα($CO_2$-$CH_4$) *vs.* reservoir temperature. Carbon isotope equilibrium (Horita, 2001) is marked by the red line. There is no indication that apparent carbon isotope fractionations vary with reservoir temperature and attain equilibrium.

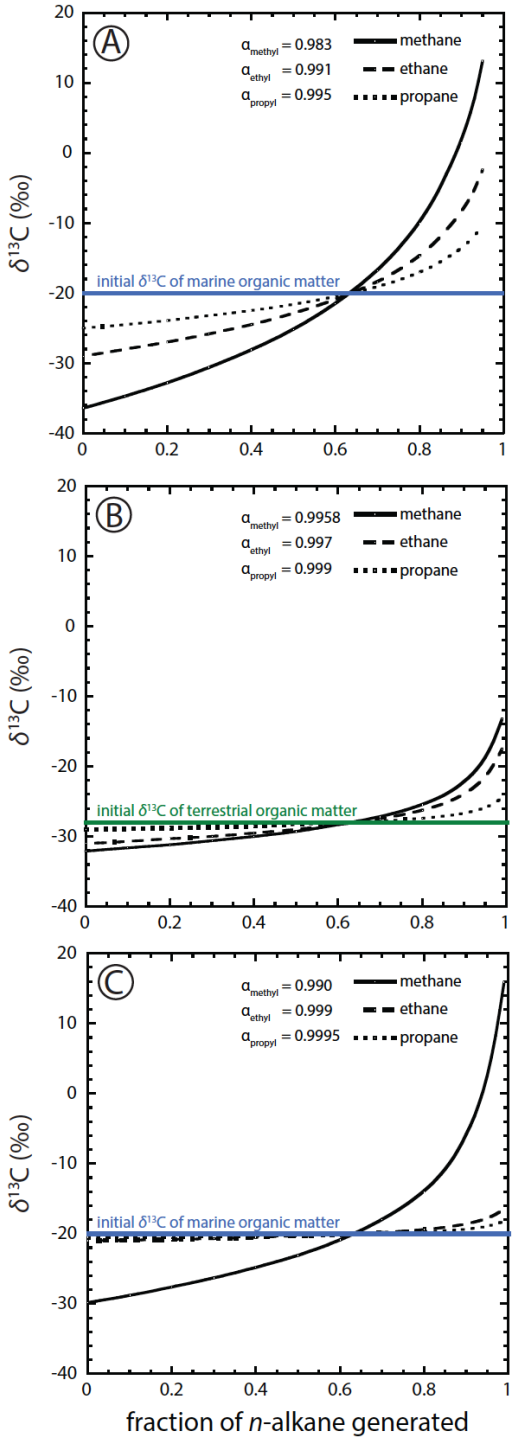


**Figure S-3** $\delta^{13}$C of instantaneous methane, ethane and propane as a function of generated fraction of *n*-alkane. Methane, ethane and propane derive from different precursor sites within the organic matter, and each generated *n*-alkane is characterised by its own specific carbon isotope fractionation factor with respect to its precursor site (for further information see Supplementary Information). During progressive cracking, instantaneous fractions of methane can become highly enriched in $^{13}$C and finally even exhibit a carbon isotope reversal with respect to ethane. **(a)** $\delta^{13}$C of the initial precursor sites corresponds with –20 ‰ to the average carbon isotopic composition of marine DOC. Carbon isotope fractionation factors between precursor sites in the organic matter and the respective *n*-alkanes correspond to those determined from pyrolysis of marine kukersite (Berner *et al.*, 1995). According to these experiments methane from marine organic matter may have the potential to become highly enriched in $^{13}$C during late stage cracking (fraction of generated methane → 1). **(b)** $\delta^{13}$C of the initial precursor sites corresponds with –28 ‰ to the average carbon isotopic composition of terrestrial $C_3$ plants. Carbon isotope fractionation factors between precursor sites in the organic matter and the respective *n*-alkanes correspond to those determined from pyrolysis of terrestrial xylite (Berner *et al.*, 1995). **(c)** $\delta^{13}$C of the initial precursor sites corresponds with –20 ‰ to the average carbon isotopic composition of marine DOC. Carbon isotope fractionation factors between precursor sites in marine organic matter and the respective *n*-alkanes chosen to match $\delta^{13}$C of Reykjanes *n*-alkanes ($\delta^{13}$C-$CH_4$ around –30 ‰; $\delta^{13}$C-$C_{2+}$ invariant and close to –20 ‰, Table S-2) at the very early stage of degassing (fraction of generated *n*-alkane → 0).

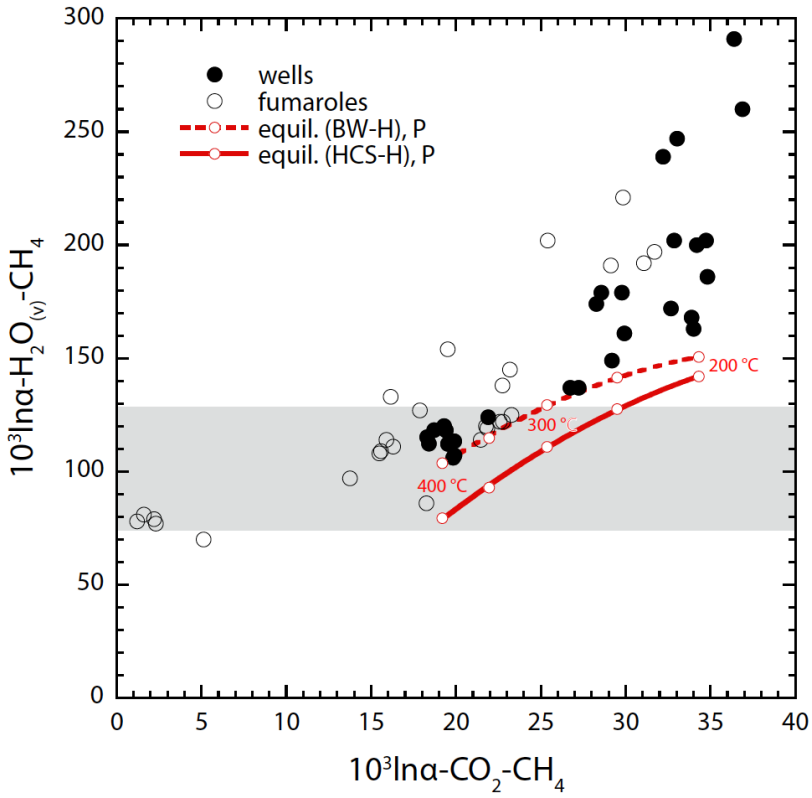


**Figure S-4** Plot of apparent carbon ($CO_2$-$CH_4$) against apparent hydrogen ($H_2O_{(v)}$-$CH_4$) isotope fractionation. For calculation of displayed equilibrium isotope fractionations see Fig. S-2 and Supplementary Information. Isotopic data for calculation of apparent isotopic fractionations are taken from Tables S-2 and S-3. The grey shaded field indicates hydrothermal temperatures ≥300 °C, *i.e.* a range within which hydrogen isotope equilibrium between $H_2O_{(v)}$ and $CH_4$ might be attained, as implied by Fig. S-2a. Within this range, the apparent hydrogen isotope fractionation between $H_2O_{(v)}$ and $CH_4$ corresponds to reasonable hydrothermal temperatures (up to 450 °C, Table S-1). Within the same range the apparent $CH_4$-$CO_2$ isotope fractionation is largely variable and extends to very small values corresponding to temperatures exceeding 1000 °C. This provides additional evidence that the apparent carbon isotope fractionation between $CO_2$ and $CH_4$ only fortuitously corresponds to equilibrium in some systems. During the stage where either the hydrogen isotopic composition of methane or that of the decomposing organic matter at depth becomes buffered by the isotopic composition of water, methane is further distilled out of the system, leaving the methane precursor sites in the organic matter and, hence, the instantaneous fractions of generated methane progressively enriched in $^{13}C$.

## *Supplementary Information References*


Abrajano, T., Sturchio, N.C., Bohlke, J.K., Lyon, G.L., Poreda, R.J., Stevens, C.M. (1988) Methane-hydrogen gas seeps, Zambales Ophiolite, Philippines: Deep or shallow origin? *Chemical Geology* 71, 211–222.

Arnórsson, S., Bjarnason, J.Ö., Giroud, N., Gunnarsson, I., Stefánsson, A. (2006) Sampling and analysis of hydrothermal fluids. *Geofluids* 6, 203–216.

Bardo, R.D., Wolfsberg, M. (1976) A theoretical calculation of the equilibrium constant for the isotopic exchange reaction between H2O and HD. *The Journal of Physical Chemistry* 80, 1068–1071.

Boschetti, T., Etiope, G., Toscani, L. (2013) Abiotic methane in the hyperalkaline springs of Genova, Italy. *Procedia Earth and Planetary Sciences* 7, 248–251.

Botz, R., Stüben, D., Winckler, G., Bayer, R., Schmitt, M., Faber, E. (1996) Hydrothermal gases offshore milos Island, Greece. *Chemical Geology* 130, 161–173.

Brombach, T., Caliro, S., Chiodini, G., Fiebig, J., Hunziker, J.C., Raco, B. (2003) Geochemical evidence for mixing of magmatic fluids with seawater, Nisyros hydrothermal system, Greece. *Bulletin of Volcanology* 65, 505–516.

Caliro, S., Chiodini, G., Moretti, Avino, R., Granieri, D., Russo, M., Fiebig, J. (2007) The origin of the fumaroles of La Solfatara (Campi Flegrei, South Italy). *Geochimica et Cosmochimica Acta* 71, 3040–3055.

Caliro, S., Chiodini, G., Paonita, A. (2014) Geochemical evidences of magma dynamics at Campi Flegrei (Italy). *Geochimica et Cosmochimica Acta* 132, 1–15.

Caliro, S., Viveiros, F., Chiodini, G., Ferreira, T. (2015) Gas geochemistry of hydrothermal fluids of the S. Miguel and Terceira Islands, Azores. *Geochimica et Cosmochimica Acta* 168, 43–57.

Chambefort, I., Buscarlet, E., Wallis, I.C., Sewell, S., Wilmarth, M. (2016) Ngatamariki geothermal field, New Zealand: Geology, geophysics and conceptual model. *Geothermics* 59, 266–280.

Chifflard, P., Fasching, C., Reiss, M., Ditzel, L. (2018) Dissolved and particular organic carbon in Icelandic proglacial streams. *The Cryosphere.* doi: 10.5194/tc-2018-32.

Chiodini, G., Cioni, R., Leonis, C., Marini, L., Raco, B. (1993) Fluid geochemistry of Nisyros island, Dodecanese, Greece. *Journal of Volcanology and Geothermal Research* 56, 95–112.

Chiodini, G. Cioni, R. Marini, L., Panichi, C. (1995) Origin of the fumarolic fluids of Vulcano Island, Italy and implications for volcanic surveillance. *Bulletin of Volcanology* 57, 99–110.

Chiodini, G., Marini, L., Russo, M. (2001) Geochemical evidence for the existence of high-temperature hydrothermal brines at Vesuvio volcano, Italy. *Geochimica et Cosmochimica Acta* 65, 2129–2147.

Chiodini, G., Avino, R., Brombach, T., Caliro, S., Cardellini, C., De Vita, S., Frondini, F., Granirei, D., Marotta, E., Ventura, G. (2004) Fumarolic and diffuse soil degassing west of Mount Epomeo, Ischia, Italy. *Journal of Volcanology and Geothermal Research* 133, 291–309.

Christenson, B.W., Mroczek, E.K., Kennedy, B.M., van Soest, M.C., Stewart, M.K., Lyon, G. (2002) Ohaaki reservoir chemistry: characteristics of an arc-type hydrothermal system in the Taupo Volcanic Zone, New Zealand. *Journal of Volcanology and Geothermal Research* 115, 53–82.

Cioni, R., Corazza, E. (1981) Medium temperature fumarolic gas sampling. *Bulletin of Volcanology* 44, 23–29.

Driesner, T. (1997) The effect of pressure on Deuterium-Hydrogen fractionation in high-temperature water. *Science* 277, 791–794.

Eirkisdottir, E.S. (2016) *Weathering and riverine fluxes in pristine and controlled river catchments in Iceland.* PhD thesis, University of Iceland.

Etiope, G., Schoell, M., Hosgormez, H. (2011) Abiotic methane flux from the Chimaera seep and Tekirova ophiolites (Turkey): understanding gas exhalation from low temperature serpentinization and implications for Mars. *Earth and Planetary Science Lett*ers 310, 96–104.

Etiope, G., Tsikouras, B., Kordella, S., Ifandi, E., Christodoulou, D., Papatheodorou, G. (2013a) Methane flux and origin in the Othrys ophiolite hyperalkaline springs, Greece. *Chemical Geology* 347, 161–174.

Etiope, G., Vance, S., Christensen, L.E., Marques, J.M., Ribeiro da Costa, I. (2013b) Methane in serpentinized ultramafic rocks in mainland Portugal. *Marine and Petroleum Geology* 45, 12-16.

Etiope, G., Judas, J., Whiticar, M.J. (2015) Occurrence of abiotic methane in the eastern United Arab Emirates ophiolite aquifer. *Arabian Journal of Geosciences* 8, 11345–11348.

Etiope, G., Vadillo, I., Whiticar, M.J., Marques, J.M., Carreira, P.M., Tiago, I., Benavente, J., Jiminez, P., Urresti, B. (2016) Abiotic methane seepage in the Ronda peridotite massif, southern Spain. *Applied Geochemistry* 66, 101–113.

Etiope, G. (2017) Abiotic methane in continental serpentinization sites: an overview. *Procedia Earth and Planetary Sciences* 17, 9–12.

Fiebig, J., Hofmann, S., Tassi, F., D'Alessandro, W., Vaselli, O., Woodland, A.B. (2015) Isotopic patterns of hydrothermal hydrocarbons emitted from Mediterranean volcanoes. *Chemical Geology* 396, 152–163.

Fontela, M., Garcia-Ibanez, M.I., Hansell, D.A., Mercier, H., Perez, F.F. (2016) Dissolved organic carbon in the North Atlantic Meridional overturning circulation. *Scientific Reports* 6, 26931.

Fritz, P., Clark., I.D., Fontes, J.C., Whiticar, M.J., Faber, E. (1992) Deuterium and $^{13}C$ evidence for low temperature production of hydrogen and methane in a highly alkaline groundwater environment in Oman. In: Kharaka, Y.K., Maest, A.S. (Eds.) *Proceedings of the 7th International Symposium on Water–Rock Interaction: Low Temperature Environments, Volume 1*. Balkema, Rotterdam, 793–796.

Fytikas, M., Karydakis, G., Kavouridis, T., Kolio, N., Vougioukalakis, G. (1990) Geothermal Research on Santorini. In: 'Thera and the Aegean World III', Volume Two: 'Earth Sciences', Proceedings of the Third International Congress. Santorini, Greece, 3-9 September 1989. Thera Foundation, 241–249.

Giggenbach, W.F. (1975) A simple method for the collection and analysis of volcanic gas samples. *Bulletin of Volcanology* 39, 15–27.

Giggenbach, W.F. (1995) Variations in the chemical and isotopic composition of fluids discharged from the Taupo Volcanic Zone, New Zealand. *Journal of Volcanology and Geothermal Research* 68, 89–116.

Gunnarsson, I., Arnórsson, S. (2000) Amorphous silica solubility and the thermodynamic properties of $H_4SiO_4$ in the range of 0 to 350 °C at $P_{sat}$. *Geochimica et Cosmochimica Acta* 64, 2295–2307.

Horibe, Y., Craig, H. (1995) D/H fractionation in the system methane-hydrogen-water. *Geochimica et Cosmochimica Acta* 59, 5209–5217.

Horita, J. (2001) Carbon isotope exchange in the system $CO_2$-$CH_4$ at elevated temperatures. *Geochimica et Cosmochimica Acta* 65, 1907–1919.

Keller, J. (1980) The island of Vulcano. *Rendiconti della Societa Italiana di Mineralogia e Petrologia* 36, 369–414.

Lopez, T., Tassi, F., Aiuppa, A., Galle, B., Rizzo, A.L., Fiebig, J., Capecchiacci, F., Giudice, G., Caliro, S., Tamburello, G. (2017) Geochemical constraints on volatile sources and subsurface conditions at Mount Martin, Mount Mageik, and Trident Volcanoes, Katmai Volcanic Cluster, Alaska. *Journal of Volcanology and Geothermal Research* 347, 64–81.

McCollom, T.M., Seewald, J.S. (2007) Abiotic synthesis of organic compounds in deep-sea hydrothermal environments. *Chemical Reviews* 107, 382–401.

Meier-Augenstein, W.M., Schimmelmann, A. (2019) A guide for proper utilisation of stable isotope reference materials. *Isotopes in Environmental and Health Studies* 55, 113–128.

Melian, G., Tassi, F., Perez, N., Hernandez, P., Sortini, F., Vaselli, O., Padron, E., Nolasco, D., Barrancos, J., Padilla, G., Rodriguez, F., Dionis, S., Calvo, D., Notsu, K., Sumino, H. (2012) A magmatic source for fumaroles and diffuse degassing from the summit crater of Teide Volcano (Tenerife, Canary Islands): a geochemical evidence for the 2004-2005 seismic-volcanic crisis. *Bulletin of Volcanology* 74, 1465–1483.

Moore, R.B. (1990) Volcanic geology and eruption frequency, Sao Miguel, Azores. *Bulletin of Volcanology* 52, 602–614.

Panichi, C., Bolognesi, L., Ghiara, M.R., Noto, P., Stanzione, D. (1992) Geothermal assessment of the island of Ischia (southern Italy) from isotopic and chemical composition of the delivered fluids. *Journal of Volcanology and Geothermal Research* 49, 329–348.

Parello, F., Allard, P., D'Alessandro, W., Federico, C., Jean-Baptiste, P., Catani, O. (2000) Isotope geochemistry of Pantelleria volcanic fluids, Sicily Channel rift: a mantle volatile end-member for volcanism in southern Europe. *Earth and Planetary Science Letters* 180, 325–339.

Potter, J., Rankin, A.H., Treloar, P.J. (2004) Abiotic Fischer-Tropsch synthesis of hydrocarbons in alkaline igneous rocks; fluid inclusion, textural and isotopic evidence from the Lovozero complex, N. W. Russia. *Lithos* 75, 311–330.

Potter, J., Longstaffe, F.J. (2007) A gas-chromatograph, continuous flow-isotope ratio mass spectrometry method for $\delta^{13}C$ and $\delta D$ measurement of complex fluid inclusion volatiles: Examples from the Khibina alkaline igneous complex, northwest Russia and the south Wales coalfields. *Chemical Geology* 244, 186–201.

Sewell, S.M., Addison, S.J., Hernandez, D., Azwar, L., Barnes, M.L. (2015) Rotokawa conceptual model update 5 years after commissioning of the 138 MWe NAP plant. *Proceedings 37th New Zealand Geothermal Workshop, 18-20 November 2015, Taupo, New Zealand*.

Sherwood Lollar, B., Frape, S.K., Weise, S.M., Fritz, P., Macko, S.A., Welhan, J.A. (1993) Abiogenic methanogenesis in crystalline rocks. *Geochimica et Cosmochimica Acta* 57, 5087–5097.

Sherwood Lollar, B., Lacrampe-Couloume, G., Slater, G.F., Ward, J., Moser, D.P., Gihring, T.M., Lin, L.H., Onstott, T.C. (2006) Unravelling abiogenic and biogenic sources of methane in the Earth's deep subsurface. *Geochimica et Cosmochimica Acta* 226, 328–339.

Stefánsson, A., Hilton, D.R., Sveinsbjörnsdottir, A.E., Torssander, P., Heinemeier, J., Barnes, J.D., Ono, S., Halldorsson, A.A., Fiebig, J., Arnorsson, S. (2017) Isotope systematics of Icelandic thermal fluids. *Journal of Volcanology and Geothermal Research* 337, 146–164.

Suda, K., Ueno, Y., Yoshizaki, M., Nakamura, H., Kurokawa, K., Nishiyama, E., Yoshino, K., Hongoh, Y., Kawachi, K., Omori, S., Yamada, K., Yoshida, N., Maruyama, S.

(2014) Origin of methane in serpentinite-hosted hydrothermal systems: The $CH_4$-$H_2$-$H_2O$ hydrogen isotope systematics of the Hakuba Happo hot spring. *Earth and Planetary Science Letters* 386, 112–125.

Suess, H. E. (1949) Das Gleichgewicht $H_2$ + HDO = HD + $H_2O$ und die weiteren Austauschgleichgewichte im System $H_2$, $D_2$ und $H_2O$. *Zeitschrift für Naturforschung* 4a, 328–332.

Taran, Y.A., Varley, N.R., Inguaggiato, S., Cienfuegos, E. (2010) Geochemistry of $H_2$- and $CH_4$-enriched hydrothermal fluids of Socorro Island, Revillagigedo Archipelago, Mexico. Evidence for serpentinization and abiogenic methane. *Geofluids* 10, 542–555.

Tassi, F., Liccioli, C., Agusto, M., Chiodini, G., Vaselli, O., Calabrese, S., Pecoraino, G., Tempesti, L., Caponi, C., Fiebig, J., Caliro, S., Caselli, A. (2016) The hydrothermal system of the Domuyo volcanic complex (Argentina): A conceptual model based on new geochemical and isotopic evidences. *Journal of Volcanology and Geothermal Research* 328, 198–209.

Tassi, F., Agusto, M., Lamberti, C., Caselli, A.T., Pecoraino, G., Caponi, C., Szentivanyi, J., Venturi, S., Vaselli, O. (2017) The 2012-2016 eruptive cycle at Copahue volcano (Argentina) versus the peripheral gas manifestations: hints from the chemical and isotopic features of fumarolic fluids. *Bulletin of Volcanology* 79: 69.